HHS Public Access

Author manuscript

J Immunol. Author manuscript; available in PMC 2022 June 15.

Published in final edited form as:

J Immunol. 2021 June 15; 206(12): 3010–3020. doi:10.4049/jimmunol.2001026.

Phosphodiesterase 10A is a key mediator of lung inflammation

Chia George Hsu[*], **Fabeha Fazal**[†], **Arshad Rahman**[†], **Bradford C. Berk**[#*], **Chen Yan**[##,*]

[*]Department of Medicine, Aab Cardiovascular Research Institute, University of Rochester School of Medicine and Dentistry, Rochester, NY, USA

[†]Department of Pediatrics, Lung Biology and Disease Program, University of Rochester School of Medicine and Dentistry, Rochester, NY, USA

[#] These authors contributed equally to this work.

Abstract

Cyclic nucleotides, cAMP and cGMP, are important regulators of immune cell functions. Phosphodiesterases (PDEs) hydrolyze cAMP and/or cGMP, and thus play crucial roles in cyclic nucleotide homeostasis. Abnormal alterations of PDE expression have been implicated in several diseases. To understand the function of PDEs in macrophages, we screened for all PDE genes in both peritoneal and alveolar macrophages from C57BL/6J mice, and found that PDE4B and PDE10A are highly induced by lipopolysaccharide (LPS). A number of PDE4 inhibitors have been used clinically for the treatment of inflammatory lung diseases. However, the role of PDE10A in inflammation is still poorly understood. We therefore investigated the role of PDE10A in macrophage inflammatory response in vitro and acute lung inflammation in vivo. We found that LPS induces a sustained PDE10A expression in macrophages, which is different from a transient induction by PDE4B. PDE10A inhibition blocked LPS-induced MCP-1 expression but not TNFα; while PDE4B inhibition blocked LPS-induced TNFα expression but not MCP1. In addition, PDE10A inhibition or deficiency decreased LPS-induced HIF-1α protein expression, and subsequently suppressed MCP1 expression. In vivo, PDE10A expression was also elevated in lung tissue after LPS exposure. Global PDE10A knockout or systemic administration of the PDE10A inhibitor TP-10 in mice, significantly suppressed inflammatory molecule levels in the lung tissue and bronchoalveolar lavage (BAL) fluid as well as inflammatory cell infiltration. These findings show that PDE10A plays a critical role in lung inflammation by promoting the activation of resident macrophages and infiltration of neutrophils.

Keywords

PDE10A; macrophage; acute lung inflammation

[#]Correspondence to: Chen Yan, Ph.D., Phone: (585) 276-7704 ; Fax: (585) 276-9829; Chen_Yan@URMC.Rochester.edu.

Author Contributions

C.G.H., F.F., A.R., B.C.B., C.Y. designed research; C.G.H. performed research; F.F., A.R., B.C.B., C.Y. contributed new reagents/analytic tools; C.G.H., B.C.B., C.Y. analyzed data; C.G.H., B.C.B., C.Y. wrote the paper.

Conflict of interest: The authors declare no conflict of interest.

Introduction

Acute lung injury and acute respiratory distress syndrome (ALI/ARDS) manifest cytokine storm and inflammatory cell infiltration. Despite decades of research, ALI/ARDS remains a major problem in intensive care unit, and the mortality of ALI/ARDS is up to 40% (1). Currently, there is no specific therapy for ALI/ARDS (2). Increasing evidence suggests that the cytokine storm, characterized by increased Interleukin-1β (IL-1β), Interleukin-6 (IL-6), monocyte chemoattractant protein-1(MCP-1), and tumor necrosis factor alpha (TNFα), leads to massive inflammatory cell infiltration that likely contributes to respiratory disease severity and outcome (3).

Cyclic nucleotides, cAMP and cGMP, are second messengers that have been shown to negatively regulate many cellular immune responses (4). Phosphodiesterases (PDEs) play critical roles in controlling cyclic nucleotide signaling by hydrolyzing cAMP and/or cGMP (5). The superfamily of PDEs is composed of 11 families with distinct substrate specificity and subcellular localization (5). For example, PDE3 and PDE4 subfamilies have been implicated in local cAMP regulation in the cardiac myocyte, which provides evidence of functional compartmentalization of PDE isoforms (6, 7). Because of the unique characteristics of each PDE isoform and their importance in many different physiologic processes, PDEs are proven drug targets for pharmacological intervention (8). Our current understanding of the PDEs that regulate inflammatory responses in macrophages and neutrophils is limited. Our preliminary screening studies have revealed that two PDEs (PDE4B and PDE10A) are predominantly upregulated by Lipopolysaccharide (LPS), a major component in gram-negative bacteria. The role of PDE4B in inflammation is well explored, which has led to the development of PDE4 inhibitors as important anti-inflammatory drugs for treating inflammatory diseases, such as psoriatic arthritis, and chronic obstructive pulmonary disease (COPD) (9, 10). However, the role of PDE10A in inflammation is still unclear.

PDE10A is able to hydrolyze both cAMP and cGMP in cell-free systems (11, 12). Under normal conditions, PDE10A expression is enriched in the striatum of brain and most studies to date have focused on the function of PDE10A in the context of neurological diseases (13). These studies have led to clinical trials using PDE10A inhibitors to treat schizophrenia and Huntington's disease (14–16). Although PDE10A expression in many peripheral tissues/cells under unstressed conditions is much lower compared to the striatum (11, 12), previous studies in cancer tissues (17–19) and our recent studies in diseased hearts (20) suggest that PDE10A expression can be induced and contribute to disease pathology. Therefore, in this study we focused on the role of PDE10A in macrophage activation and acute lung injury after LPS exposure. Our findings indicate that PDE10A induction plays a causative role in inflammatory molecule expression and acute lung inflammation.

Materials and Methods

Reagents

Medium: Dulbecco's modified eagle medium (MT-10-013-CV), Fetal bovine serum (10437-028), RPMI 1640 medium (11875-093), Sodium pyruvate (11360070), and

Streptomycin/penicillin (15140-122) were from Thermo Fisher Scientific (MA, USA). ECGS (E9640) was from BioMedical Technologies Inc (MA, USA). Low Serum Growth Supplement (S-003-010), and Media M200 (M200-500) were from Cascade Biologics (OR, USA). 2-Mercaptoethanol (M7522) was from Sigma-Aldrich (MO, USA). Chemical: ABC-HRP conjugate (PK-6100), Mouse on Mouse (M.O.M.™) Blocking Reagent (MKB-2213), and Normal horse serum (S-2000) were from Vector Laboratories (CA, USA). Bio-Gel® P Polyacrylamide Beads (1504114) were from Bio-Rad Laboratories (CA, USA). Citrate Buffer pH 6.0, 10x (21545) and Immobilon Western Chemiluminescent HRP (WBKLS0500) Substrate were from EMD Millipore (MA, USA). Collagenase Type I (LS004196) was from Worthington biochemical corporation (NJ, USA). Cell Lysis Buffer (10X) (9803s) was from Cell Signaling Technology (MA, USA). DAPI Fluoromount-G (0100-20) was from SouthernBiotech (AL, USA). DAB HRP Substrate (K-3468) was from DAKO (ON, Canada). Dimethyl sulfoxide hybrid-max sterile (D2650), Lipopolysaccharides from Escherichia coli (L3129), Heparin (H3149-25KU), Roflumilast (162401-32-3), Protease inhibitor cocktail (P8340), and Sodium fluoride (S6521)were from Sigma-Aldrich (MO, USA). EDTA solution (BP24831), Hydroxypropyl-β-cyclodextrin (297560250) and Low-melting point agarose (16520100) were from Thermo Fisher Scientific (MA, USA). Ketamine (K0001) was from SMH Pharmacy (NY, USA). Normal mouse IgG (sc-2025) was from Santa Cruz Biotechnology (TX, USA). RTL lysis buffer (79216) was from Qiagen (Hilden, Germany). Saline (2F7123) was from Cardinal Health (OH, Ireland). TP-10 (Gift) was from Pfizer (NY, USA). Xylazine (005469) was from Bimeda (IL, USA). IDF-11774 was from MedChem Express. Assay kit: Bicinchoninic acid (BCA) kit (BCA-1) was from Pierce (IL, USA). iScript™ cDNA Synthesis Kit (1708891) and iQ™ SYBR® Green Supermix (1708882) were from Bio-Rad Laboratories (CA, USA). MCP-1 (RUO 432704), TNFα (RUO 430904), IL-1β (RUO 432604) and IL-6 (RUO 431304) ELISA kits were from BioLegend (CA, USA). Antibody: Alexa Fluor 488 Goat Anti-rabbit IgG(H+L) highly cross-adsorbed (A-11034) was from Molecular Probes (OR, USA). Anti-mouse IgG, HRP-linked Antibody (7076), Anti-rabbit IgG, HRP-linked Antibody (7074), β-actin antibody (4967), NF-kB p65 (D14E12) and Phospho-NF-κB p65 (Ser536) (93H1) were from Cell signaling (MA, USA). HIF-1α Antibody (GTX127309 was from GeneTex. Biotinylated goat anti-mouse IgG (BP-9200-50) was from Vector Laboratories (CA, USA). Dynabeads Sheep anti-Rat IgG (110-35) and MPO antibody (PA5-16672) were from Thermo Fisher Scientific (MA, USA). PDE10A antibody (sc-515023) was from Santa Cruz Biotechnology (TX, USA). Rat anti-mouse PECAM-1 specific antibody (553370) was from BD Pharmingen (CA, USA).

Animal

Age of 10–12 weeks female and male mice were used in the experiments. PDE10A knockout on a C57BL/6J background and littermate controls were used for all experiments. The PDE10A knockout mice were originally obtained from Jackson Laboratory. All mice were housed in a specific pathogen-free facility and kept in a temperature-controlled room set to a light and dark cycle of 12 hours each. The mice had ad libitum access to standard mouse chow and water. All of the experiments were approved by the University Committee on Animal Use For Research (UCAR) at the University of Rochester and followed National Institutes of Health guidelines for experimental procedures on mice.

Oropharyngeal administration of LPS

Age and background matched PDE10A-WT and PDE10A-KO female or male mice between 10–12 weeks of age were anesthetized with ketamine (40 mg/kg) /xylazine (3 mg/kg). After respiratory rate was significantly decreased, the mouse was suspended by a rubber band on a 60° incline board. The oral cavity was exposed and the tongue was fully extended by forceps. Using a P200 micropipette, physiological saline alone or 0.2 mg/kg LPS (Escherichia coli O127:B8) diluted in saline was instilled into the oropharyngeal space of mice. Occlusion of the nose for 5 seconds and the tongue were extended following clearance of the liquid from the oropharynx. Animals were subsequently removed from the board and observed closely until fully recovered from anesthesia.

LPS inhalation in vivo

Age and background matched PDE10A-WT and PDE10A-KO female or male mice between 10–12 weeks of age were used for LPS inhalation. Mice were randomly placed in stainless steel compartments inside a polycarbonate rectangular chamber connected to a nebulizer on one side and a vacuum system on the other side. The dose and duration of LPS exposure were based on previous studies (21). LPS (10mg/10mL saline) solution was aerosolized into the chamber for 30 minutes. Control mice were given aerosolized saline solution. Mice will be removed from the chamber after complete aerosolization and returned to the room (21). Whole-body inhalation exposures do not cause pain or distress in mice. Furthermore, animals were monitored throughout exposure. For TP-10 treatment, TP-10 was dissolved in a vehicle consisting of 10% DMSO and 40% hydroxypropyl-β-cyclodextrin based on previous studies (15, 20). C57BL/6J mice were randomized to receive TP-10 (6 mg/kg) or vehicle (10% DMSO in 40% β-cyclodextrin v/v) administered subcutaneously one hour before exposure (15). We did not observe any side effect after 24 hours TP-10 treatment.

Peritoneal macrophage isolation

Peritoneal macrophage isolation was performed as previously described (22, 23). Bio-Gel preparation: Wash Bio-Gel P-100 gel three times with PBS. Pellet Bio-Gel by centrifugation for 5 min at 400 × g, then resuspend in PBS to yield 2% (w/v) Bio-Gel. Autoclave for 20 min before use. PDE10A knockout mice and their littermate control were used. Peritoneal macrophages were harvested on age and background matched PDE10A-WT and PDE10A-KO female or male mice between 10–12 weeks of age. Mice received intraperitoneal injection (IP) of 1mL 2% fine polyacrylamide beads. On four days after injection, the animals were euthanized by CO_2 and macrophages were harvested by washing their peritoneal cavity with 5 mL ice-cold PBS supplemented with 1mM EDTA. The cell suspension was centrifuged at 500 g for 5 min at 4°C, and the supernatant was discarded. The cell pellet was washed one time in PBS and the supernatant was removed through centrifugation. The cell pellet was suspended in RPMI 1640 medium supplemented with 10% FBS, 1% streptomycin/penicillin, 0.1mM 2-Mercaptoethanol, and 1mM sodium pyruvate. Macrophages were cultured at 1.6×10^5 cells/well on 12-well plates. After incubated for 2 hours, cells were washed twice with PBS and media was replenished. Cells were used for experiments after 24 hours of culture.

Alveolar macrophage isolation

Alveolar macrophage isolation was performed as previously described (22). Alveolar macrophages were harvested on PDE10A-WT or PDE10A-KO mice between the age of 10–12 weeks. Mice were euthanized via CO_2. The upper part of the trachea was cannulated with a catheter IV (Medline Industries, IL, B-D381134Z) and then lavaged 10 times with 1 mL of PBS supplemented with 1 mM EDTA. BAL fluid was centrifuged at 500 × g for 5 min at 4°C. Macrophages were cultured at 0.8×10^5 cells/well on 12-well plates in 1640 medium supplemented with 10% FBS, 1% streptomycin/penicillin, and 1mM sodium pyruvate. Cells were used for experiments after 24 hours of culture.

MLMEC isolation

C57BL/6J (10–12 weeks old) mice were anaesthetized with a single intraperitoneal injection of ketamine (130 mg/kg) and xylazine (8.8mg/kg). Saline perfusion was performed to eliminate the blood cells. Lungs were harvested and mouse lung microvascular endothelial cells (MLMECs) were isolated by using immunoselection method as previously described (24). Lungs were removed and digested in PBS supplemented with collagenase type I for 40 min at 37 °C, followed by filtration with 70 μm strainers. Lung endothelial cells were then isolated using magnetic beads (dynabeads sheep anti-rat IgG) pre-coated with purified rat anti-mouse pecam-1 specific antibody. MLMECs were maintained in DMEM containing 20% FBS, 10 mg/L ECGS, 40 mg/L heparin and 1X streptomycin/penicillin until 80% confluent (5–7 days). Cells were passaged and seeded at 1×10^4 cells/well on 12-well plate. Cells were used for experiments after 2 days of culture.

HUVEC isolation

HUVEC (Human Umbilical Vein Endothelial Cells) isolation from human umbilical cord was performed as previously described (24). Four donated umbilical cord veins were digested with collagenase type I (1mg/mL) for 20 min at 37C, centrifuge ~10min at 4°C 1000rpm and cultured in complete media M200 5% FBS 1% streptomycin/penicillin and 2% LSGS. Cells from liquid nitrogen were frozen down at Passage 2–3.

LPS stimulation in vitro

To stimulate the peritoneal macrophages or alveolar macrophages, cultures were rinsed twice with serum and antibiotic-free RPMI 1640 medium. The medium was replaced with fresh RPMI 1640 medium with 1mM sodium pyruvate. To stimulate the MLMEC and HUVEC, cultures were rinsed twice with serum and antibiotic-free DMEM medium. The medium was replaced with fresh DMEM medium. In dose experiments, all wells were exposed to LPS (1–500ng/mL) for 6 or 24 hours, as indicated. For time-course studies, individual wells were exposed to LPS (100ng/mL) for different times, but to minimize manipulation of each plate, the total incubation time was 24 hours for all treatment groups.

Collection of BAL fluid and lung tissue

Mice were anesthetized via intraperitoneal injection of ketamine /xylazine before euthanasia via cervical dislocation. The upper part of the trachea was cannulated and then lavaged with 1 mL followed by 0.5 mL of PBS supplemented with 1 mM EDTA. BAL fluid

was centrifuged at 500 × g for 5 min at 4°C. bronchoalveolar lavage (BAL). Total cell counts in the BAL fluid were determined with a hemocytometer. The cell differentials in the BAL fluid were determined using cytocentrifuge preparations stained with HEMA 3 and by examining 200 cells under a microscope. BAL fluids were analyzed for cytokines and chemokine. The superior lobe, and inferior lobe were snapped frozen in liquid nitrogen to quantify gene expression, and protein expression, respectively. Superior lobe was homogenized in RTL lysis buffer. Inferior lobe was homogenized in cell lysis buffer supplemented with 5 mM sodium fluoride and protease inhibitor cocktail. Protein levels were measured by BCA kit.

Immunohistochemistry and immunofluorescence of lung tissue

Lungs were harvested from mice that did not undergo lavage. Mice were anesthetized via intraperitoneal injection of ketamine /xylazine. The lungs were perfused free of blood by gentle infusion of 10 ml PBS containing 1 mM EDTA through right ventricle. Lungs were inflated with 2mL warm (50°C), PBS-equilibrated 2% low-melting point agarose and poured ice on top to stiffen the lung tissues. Lung tissues were removed, drop fixed in 60% methanol, 30% water, and 10% acetic acid, embedded in paraffin, cut into 5 μm sections, and mounted onto slides. Sections were deparaffinized before use. For Immunohistochemistry, sections were treated with 3% H_2O_2 for 10 minutes at room temperature followed by antigen retrieval for 20 minutes with steam using 1X Citrate buffer, pH=6.0. Sections were blocked in PBS with 10% normal horse serum and Ig Blocking Reagent (M. on M. kit) for 1 hour at room temperature followed by overnight incubation at 4°C with PDE10A antibodies (1:200) in 2% normal horse serum diluent. Sections were then incubated with biotinylated horse anti-mouse IgG (1:500) in 2% normal horse serum diluent for 1 hour at room temperate followed by three times washing with PBS. ABC-HRP conjugate was used in conjunction with the chromogenic HRP substrate/reagent DAB. Finally, nuclei were counterstained with hematoxylin. As a negative control, adjacent sections were incubated with a mouse IgG with the primary antibody omitted. Whole brain sections from mouse were stained for positive controls. For immunofluorescence, sections were treated with 3% H_2O_2 for 10 minutes at room temperature followed by antigen retrieval for 20 minutes with steam using 1X Citrate buffer, pH=6.0. Sections were blocked in 10% normal goat serum in PBS for 1 hour at room temperature followed by overnight incubation at 4°C with MPO antibodies (1:500) in 2% normal goat serum in PBS. Fluorescence-conjugated secondary antibodies (1:1000) were incubated for 1 hour at room temperature and followed by three times washing with PBS. Nuclei were counterstained with 4’,6-diamidino-2-phenylindole (DAPI, fluoromount-G). Fluorescent images were captured by a confocal microscope (Olympus BX51, Software: SPOT Imaging software advanced). MPO and DAPI positive cells were quantified by using NIH ImageJ software.

P65 translocation

p65 nuclear translocation was detected by immunofluorescence staining using a p65 antibody and DAPI. Peritoneal macrophages were seeded on glass coverslips in 12- well plates and treated with LPS for 24 hr. Cells were washed twice with cold PBS and fixed with 4% formaldehyde in PBS for 10 min. After washing with PBS, the cells were incubated

with blocking solution (10% normal goat serum, and 0.1% Triton X-100 in PBS) for 1 h followed by incubating with the p65 antibody (1:500) overnight. The next day, cells were washed three times with PBS and incubated with the anti-rabbit secondary antibody (Alexa Fluor 488) for 1 h in PBS in the dark. After washing three times with PBS, samples were mounted using fluoromount-G. Immunofluorescence was analyzed by confocal microscope. p65 nuclear translocation was evaluated using NIH ImageJ software with an intensity ratio nuclei cytoplasm tool. Quantification of p65 translocation was expressed as the percentage of p65 intensity in nucleus over total cell (25). At least 6 images were quantified for each experimental group.

Cytokine assay

BALF and lung tissue levels of cytokine were determined by Eve Technology (AB, Canada) using cytokine array (MDF10). MCP-1, IL-6 and IL-1β levels were confirmed by ELISA kits according to the manufacturer's instructions. For in vitro studies, culture media was collected immediately after treatment. Samples were cleared by centrifugation at 16k×g for 5 min and stored at −20 °C. MCP-1, IL-6, and TNFα were measured in supernatants with ELISA kits.

RNA extraction and Real-time PCR

Complimentary DNA was synthesized from 0.1μg (cell) or 0.5μg (tissue) RNA by reverse transcription. Amplification reactions contained a target specific fraction of the reverse transcription product and 1 μM forward and reverse primers in SYBR Green QPCR master mix. Fluorescence was monitored and analyzed in a CFX connect real-time PCR system. Gene expression was normalized by β-actin and an independent reference sample using delta delta CT method. Amplification of specific transcripts was confirmed by melting curve analysis at the end of each PCR experiment. The mouse and human primers are shown below. Human β-actin (Forward: CATGTACGTTGCTATCCAGGC, Reverse: CTCCTTAATGTCACGCACGAT); Human PDE10A (Forward: GAAGAGTGGCAAGGTCTCATGC, Reverse: ATGTCCCACAGGACCGATGAAC); Mouse β-actin (Forward: TTCAACACCCCAGCCATGT, Reverse: GTAGATGGGCACAGTGTGGGT); Mouse PDE1B (Forward: GAGCCAACCTTCTCTGTGCTGA Reverse: CGTCCACATCTAAAGAAGGCTGG); Mouse PDE1C (Forward: CAGTCATCCTGCGAAAGCATGG, Reverse: CCACTTGTGACTGAGCAACCATG); Mouse PDE2A (Forward: ACGCGCAACATTCTCTGCTTCC Reverse: TGCCACAGTAGATGGAGAAGGC); Mouse PDE3A (Forward: ATACCTGCTCGGACTCTGAGGA, Reverse: TGGCAGAGGTGGTAGTTGTCCA); Mouse PDE 3B (Forward: GAGGTCATCGTCTGTGTCACTG, Reverse: GTTAGAGAGCCAGCAGACACTG); Mouse PDE 4A (Forward: CCGTGTTCACAGACCTGGAGAT, Reverse: GGTGGTTCTCAAGCACAGACTC); Mouse PDE 4B (Forward: ATGAGCCTCCTGGCAGACCTTA, Reverse: CTGCACAGTGTACCATGTTGCG); Mouse PDE 4D(Forward: CACCAGCACTTAGAGGAGAAGAG, Reverse: CTCTGCGTTCTCAAGGCAAAGG); Mouse PDE 5A (Forward: GAGCAGTTCCTGGAAGCCTTTG, Reverse: CGCTGATGCATGGTAAGACAGG); Mouse PDE 6A (Forward: TGGTGAAGTGCGGCATCCAGAT, Reverse:

ATGCCGCCAGTTGTGGTAAGTG); Mouse PDE 6C (Forward: GGACCAAAGACTCCAGATGGCA, Reverse: GGCAATCCACTAACAAGCGTCC); Mouse PDE 6D (Forward: GCAGAACAAATGGAAAAATTCCGC, Reverse: AAGGACTGCCAGGTGTTTGTGG); Mouse PDE 7A (Forward: AATTGCAGCCGCCACTCACGAT, Reverse: CCAGTGGTGATTCTCCAGGACT); Mouse PDE 8A (Forward: CCAAAGCGGTTTCCTCCAGAAC, Reverse: GGACTGTTTTCCTGGGCAGCAT); Mouse PDE 10A (Forward: ACTGGAAGCATGCAGTCAC, Reverse: ACACCGTCTGGGAGAAGT); Mouse PDE 11A (Forward: CGTGTTCCAAGGCTGAAGTCGA, Reverse: ATCCGTAGAGCGGCTGTGATCA); Mouse MCP-1 (Forward: AGGTCCCTGTCATGCTTCTG, Reverse: TCTGGACCCATTCCTTCTTG); Mouse IL-1β (Forward: GAGTGTGGATCCCAAGCAAT, Reverse: ACGGATTCCATGGTGAAGTC); Mouse IL-6 (Forward: GAGGATACCACTCCCAACAGACC, Reverse: AAGTGCATCATCGTTGTTCATACA); Mouse TNFα (Forward: TCTTCTCATTCCTGCTTGTGG, Reverse: GGTCTGGGCCATAGAACTGA); Mouse GLUT1 (Forward: GGTTGTGCCATACTCATGACC, Reverse: CAGATAGGACATCCAGGGTAGC); Mouse HK1 (Forward: GTGGACGGGACGCTCTAC, Reverse: TTCACTGTTTGGTGCATGATT).

Western blot

To assay protein level, soluble protein (20 μg from lung samples and 4 μg from cell lysates) was separated by SDS-PAGE through 10 % acrylamide gels. Protein was transferred to nitrocellulose membranes, blocked with 5 % nonfat dry milk in Tween-TBS and hybridized with indicated antibody (PDE10A 1:1000; phospho-p65 1:1000; HIF-1α 1:1000; β-actin 1:4000) overnight. Membranes were rinsed and incubated with horseradish peroxidase conjugated secondary antibody. Bands were detected by enhanced chemiluminescence, visualized by exposure to radiographic film, quantified by scanning densitometry, and normalized to the β-actin. Brain tissue homogenates from mouse were used as positive controls for PDE10A.

Statistics

Unless otherwise noted, in vitro experiments were repeated as three independent procedures, with duplicate or triplicate wells averaged prior to statistical analysis. All data were presented as mean ± SEM. GraphPad Prism 8.0 was used for statistical analysis. Comparisons between two groups after LPS exposure were analyzed by two-way ANOVA. TP-10 and roflumilast experiments in cell cultures were analyzed by one-way ANOVA followed by post hoc T tests using Bonferroni correction for multiple comparisons. P values were indicated as follow: * < 0.05, ** < 0.01, *** < 0.001, **** < 0.0001.

Results

LPS differentially upregulates PDE10A and PDE4B expression in macrophages in vitro.

Alveolar macrophages are the lung's first line of defense against infection. Acute lung injury is directly correlated with the macrophage activation status (26). Peritoneal macrophages are widely used for studies of macrophage inflammation (23, 27, 28). Therefore, we studied

PDE10A expression in both alveolar and peritoneal macrophages. We first examined all PDE genes in macrophages after LPS stimulation for 6 hours and found the expression levels of two PDEs were predominantly and markedly upregulated. LPS significantly upregulated PDE4B and PDE10A expression in peritoneal and alveolar macrophages (Fig. 1A). The effects of LPS on expression of other PDEs were minimal (Fig. 1A). Importantly, LPS stimulation of PDE4B and PDE10A expression exhibited different time courses. LPS-induced PDE4B expression was faster and transient with peak around 1 hour and decreased to near baseline by 6 hours (Fig. 1B). However, LPS-induced PDE10A expression was relatively slower and sustained with the peak around 3 hours and remained high for the duration of 24 hours (Fig. 1B). LPS upregulated PDE10A expression in a dose-dependent manner in alveolar and peritoneal macrophages (Fig. 1C). LPS did not stimulate PDE10A expression in mouse lung microvascular endothelial cells (MLMEC) and in human umbilical vein endothelial cells (HUVEC) (Fig1. C).

PDE10A and PDE4B inhibition have differential effects on LPS-induced cytokine expression in macrophages in vitro.

Based on the time courses of PDE10A and PDE4B induction by LPS, we hypothesized that PDE10A and PDE4B may regulate the expression of different inflammatory molecules. Indeed, we found that LPS induced a transient TNFα gene expression that peaked at 6 hours and declined by 24 hours (Fig. 2A). In contrast to TNFα, LPS-induced mRNA expression of MCP-1 and IL-6 was gradually and continually increased over 24 hours (Fig. 2B and Supplemental Fig. S1A). Interestingly, the PDE4B inhibitor roflumilast, but not the PDE10A inhibitor TP-10 drastically reduced TNFα mRNA levels assessed by RT-PCR (Fig. 2C and supplemental Fig. S2A and S2C). Roflumilast also decreased secreted TNFα assessed by ELISA (Fig 2D) in peritoneal macrophages stimulated by LPS. In contrast, TP-10, but not roflumilast, significantly reduced LPS-induced MCP-1 mRNA levels (Fig. 2E, and Supplemental Fig. S2B and S2D) as well as MCP-1 secretion (Fig. 2F). Similar results were obtained in IL-6 mRNA expression and secretion in TP-10 treated or PDE10A-KO macrophages compared to controlled macrophages (Supplemental Fig. S1B–C). These results indicate that the effects of PDE4B and PDE10A inhibition on inflammatory molecule expression are consistent with the time course of PDE4B and PDE10A induction by LPS.

PDE10A knockout reduces LPS-mediated MCP-1 mRNA and secreted protein level in macrophages in vitro.

PDE10A inhibitor TP-10 exhibited an inhibitory effect on MCP-1 mRNA expression and protein secretion (Fig. 2). We next examined the effects of genetic depletion of PDE10A on MCP-1 expression. We isolated peritoneal macrophages from PDE10A wild-type mice (PDE10A-WT) and global knockout (PDE10A-KO) mice and stimulated them with LPS. As we anticipated, LPS-induced MCP-1 mRNA levels were significantly reduced in PDE10A-KO macrophages compared to PDE10A-WT macrophages (Fig. 3A). Consistently, MCP-1 secretion was also significantly decreased in PDE10-KO macrophages (Fig.3B). To determine the specificity of TP-10, we compared the effects of TP-10 in PDE10-WT and PDE10A-KO macrophages. TP-10 treatment significantly reduced LPS-stimulated MCP-1 production in PDE10A-WT macrophages, but there were no significant effects in the PDE10A-KO macrophages (Fig. 3C). This indicates that the effect of TP-10 on MCP-1

production is by inhibiting PDE10A. Likewise, PDE10A knockout or inhibition by TP-10 also significantly reduced LPS-induced MCP-1 mRNA levels in alveolar macrophages (Fig 3D–E).

PDE10A inhibition or knockout reduces HIF-1a expression in macrophages after LPS treatment.

To identify the key mediator that links PDE10A and inflammatory molecules. We first focused on the nuclear factor kappa-light-chain enhancer of activated B cells (NF-κB), a key transcriptional factor involved in regulating expression of proinflammatory molecules. Phosphorylation and nuclear translocation of p65 regulates NF-κB Activity. Therefore, we evaluated the role of PDE10A in p65 phosphorylation, and p65 nuclear translocation after LPS treatment in peritoneal macrophages. We did not find any significant difference in LPS-induced p65 phosphorylation between DMSO and TP-10 treated macrophages (Supplemental Fig. S3A) or between PDE10A-WT and PDE10A-KO macrophages (Supplemental Fig. S3B) after LPS stimulation. Consistently, TP-10 treated macrophages did not change LPS-induced p65 nuclear translocation in peritoneal macrophages compared to DMSO-treated cells (Supplemental Fig. S3C–D).

In our recent RNA-sequencing data in the whole heart, we found that PDE10A regulated cytokine production pathway, and hypoxia-inducible factor 1-alpha (HIF-1α) signaling pathway during heart failure pathogenesis (20). Previous studies have revealed that HIF-1α is a transcription factor required for glycolytic adaptation, macrophage activation and pro-inflammatory phenotype following LPS stimulation (29, 30). Therefore, we analyzed HIF-1α protein expression and the mRNA expression of HIF-1α target genes, such as glucose transporter-1 (GLUT1) and hexokinase-1 (HK1) in macrophage. We found that PDE10A knockout or inhibition by TP-10 significantly decreased LPS-induced HIF-1α protein expression in macrophages (Fig.4A and 4E). GLUT1 and HK1 gene expressions were also down-regulated in TP-10 treated or PDE10A-KO macrophages compared to control groups after LPS stimulation (Fig.4B–C and 4E–F). To determine the role of PDE10A and HIF-1α in cytokine production, we measured MCP-1 secretion in PDE10-WT and PDE10A-KO macrophages with or without HIF-1α inhibitor, IDF-11774. IDF-11774 treatment significantly reduced LPS-stimulated MCP-1 production in PDE10A-WT macrophages, but IDF-11774 treatment had no effect on MCP-1 production in PDE10A-KO cells (Fig. 4D). Likewise, IDF-11774 treatment reduced MCP-1 production in DMSO-treated macrophages, but not in TP-10 treated macrophages after LPS stimulation (Fig. 4H). These results indicate that HIF-1α may act downstream of PDE10A in LPS-stimulated MCP-1 production.

LPS exposure induces PDE10A expression in mouse lung

The LPS exposure mouse model has been used to explore mechanisms of human lung diseases and to discover new drug targets (21, 31). Given the role of PDE10A in MCP-1 production, we next tested whether PDE10A regulates acute lung injury in mice exposed to LPS by two different routes, oropharyngeal delivery and inhalation. Endotoxins, such as LPS, have been used to induce ALI/ARDS. To determine PDE10A expression in lung after acute lung injury, C57BL/6J mice were exposed to LPS by inhalation and lung tissues were

harvested at 6 hours to detect PDE10A expression. LPS significantly increased PDE10A mRNA (Fig.5A) and protein levels (Fig.5B). By using immunohistochemical analysis of lung tissue, we observed that PDE10A expression was low in mice after saline treatment, but PDE10A positive cells were increased in alveolar space (Fig.5C) after LPS exposure. This result suggests that PDE10A expression is highly induced in infiltrated cells.

PDE10A knockout mice exhibit decreased lung inflammation after oropharyngeal delivery of LPS

To investigate the role of PDE10A in lung inflammation in vivo, PDE10A-WT and PDE10A-KO mice were exposed to a single dose of LPS (0.2 mg/kg) by oropharyngeal delivery. BAL fluid and lung tissues were collected to assess the inflammatory response 24 hours after exposure. Total cell number significantly increased 24 hours after LPS administration in PDE10A-WT mice, whereas PDE10A-KO significantly reduced total cell number compared to PDE10A-WT mice (Fig. 6A). Polymorphonuclear neutrophil (PMN) infiltration plays an important role in the progression of ALI. To determine the role of PDE10A in neutrophil infiltration after LPS, the number of neutrophils compared to total cells in the BAL fluid was evaluated by cell count and morphology as described in methods. The results show that alveolar macrophages were the major resident white blood cells in the alveoli. LPS exposure significantly increased total cell number and induced neutrophil infiltration in PDE10A-WT mice (Fig. 6B–C). The percentage of neutrophils was significantly lower in PDE10A-KO mice as compared to PDE10A-WT (Fig. 6B–C). To further confirm the role of PDE10A in lung inflammation, BAL fluid and lung homogenate samples were examined by ELISA and Real Time-PCR for inflammatory cytokine measurement. Consistently, MCP-1 and IL-6 protein levels in BAL fluid and mRNA levels in lung tissues were lower in PDE10A-KO than in PDE10A-WT mice after LPS stimulation (Fig. 6D–G).

PDE10A knockout attenuates lung inflammation in mice after LPS inhalation.

LPS inhalation model provides a more natural route of entry into the host respiratory tract than oropharyngeal delivery, and is therefore a more physiological exposure. To investigate the role of PDE10A in lung inflammation from airborne LPS, PDE10A-WT and PDE10A-KO mice were exposed to LPS for 30 minutes in stainless steel compartments inside a polycarbonate rectangular chamber. Control mice were given aerosolized saline solution (21). Lung tissues and BAL fluid were harvested at 18 and 24 hours after exposure. We first analyzed 10 different cytokine protein levels in lung tissues and bronchoalveolar lavage (BAL) fluid by cytokine array. LPS markedly induced IL-1β, MCP-1, IL-6 and TNFα protein levels in lung tissues from PDE10A-WT mice, which were significantly attenuated in lung tissues from PDE10A-KO mice (Table 1). In BAL fluid, MCP-1 and IL-6 levels were also significantly lower in in PDE10A KO mice compared to PDE10A-WT mice (Table 1). Consistently, MCP-1, IL-6 and IL-1β mRNA levels in lung tissues were lower in PDE10A-KO than in PDE10A-WT mice after LPS stimulation (Fig. 7A–C and Supplemental Fig 4A–E).

Next, we examined inflammatory cell infiltration using myeloperoxidase (MPO) staining, an enzyme present in neutrophils and macrophages (32). LPS inhalation increased MPO

positive cells in the lung tissue demonstrating neutrophils and macrophages infiltration. Consistent with cytokine data, there were significantly fewer MPO positive cells in lung tissue from PDE10A-KO mice than in PDE10A-WT mice (Fig 7D–E). These data show that PDE10A deficiency reduces inflammatory cell infiltration and cytokine secretion in the lung after LPS exposure.

PDE10A inhibition reduces LPS-induced lung inflammation.

The PDE10-specific inhibitor, TP-10, has been administered systemically in pre-clinical models of schizophrenia (14, 15), as well as in mouse models of heart failure (20). Next, we determined whether TP-10 treatment is sufficient to reduce LPS-induced lung inflammation. We injected TP-10 (6mg/kg), subcutaneously in mice 1 hour prior to LPS inhalation. Protein levels of IL-1β and IL-6 in BAL fluid and MCP-1 protein level in lung tissue were significantly lower in TP-10 treated group as compared to vehicle treatment (Fig. 8A–C). Notably, LPS inhalation significantly induced MPO positive cells in the lungs of WT mice treated with vehicle, which was significantly reduced in mice treated with TP-10. (Fig. 8D–E). Again, our findings indicate that PDE10A inhibition by TP-10 is able to reduce lung inflammation after the exposure to LPS.

Discussion

There are three major key findings in the present study. First, LPS stimulation resulted in PDE10A up-regulation in vitro macrophages and in lung tissues. Second, PDE10A regulated MCP-1 secretion in macrophages. Third, PDE10A deficiency or inhibition reduced lung inflammation in two mouse models of LPS exposure. Acute lung injury (ALI) is a syndrome characterized by massive cytokine secretion and inflammatory cell infiltration. Our present data suggest that PDE10A is a key mediator of lung inflammation and cytokine secretion, and inhibition of PDE10A is useful for the control of the pathogenesis of ALI; especially due to severe inflammation.

Using genetic and pharmacological approaches, we found that PDE10A contributes to LPS-induced MCP-1 mRNA and secreted protein in peritoneal macrophages and alveolar macrophages (Fig. 3). Interestingly, PDE10A inhibition by TP-10 had no effect on LPS-induced TNFα expression (Fig. 2). Different from PDE10A inhibition, we found that PDE4B inhibition by roflumilast suppressed LPS-induced TNFα but not MCP-1 in macrophages (Fig. 2). In a previous study, roflumilast reduced LPS-induced TNFα in alveolar macrophages from COPD patients whereas MCP-1 was not affected (33), which is similar to our findings. We believe that the differential effects of PDE10A and PDE4B inhibition on LPS-induced TNFα and MCP-1 are likely due to the different time courses of LPS-increased PDE10A and PDE4B expression. LPS stimulated a quick and transient induction of PDE4B (Fig.1), which was synchronous to TNFα induction by LPS (Fig. 2). LPS stimulated a slower and sustained induction of PDE10A (Fig. 1), which was consistent with a gradual and continuous MCP-1 induction by LPS (Fig. 2). Thus, it is possible that PDE4B may be responsible for certain early induced inflammatory molecules, while PDE10A is required for the later induction of inflammatory molecules in macrophages

upon LPS stimulation. The roles of PDE10A and PDE4B in regulating other inflammatory molecules deserve to be further investigated.

NF-kB is a transcription factor that stimulates multiple proinflammatory mediators (34–36). A previous study showed that PDE10A inhibition by papaverine exerted anti-inflammatory effect through inhibiting NF-κB pathway in the BV2 microglial cell line (13). Papaverine is not a selective inhibitor for PDE10A because the IC_{50} values of papaverine for PDE3 and 4 inhibition are less than 10 folds compared to the IC_{50} value for PDE10A (37). Indeed, papaverine has shown off-target effects in animals (38). In our current study, we used genetically engineered PDE10A knockout mice and much more specific pharmacological inhibitor TP-10. We found that neither TP-10 treatment nor PDE10A knockout could inhibit p65 phosphorylation and its nuclear translocation after LPS stimulation in peritoneal macrophages. NF-kB signaling is rapidly activated by LPS (39), and NF-kB signaling is important in PDE4B-mediated inflammatory response (40). The transient nature of NF-kB signaling may explain that PDE4B but not PDE10A connects to the NF-kB signaling. Since LPS induced a delayed but sustained induction of PDE10A, which was consistent with a gradual and continuous MCP-1 induction by LPS. We believe that the mechanisms contributing to PDE10A-mediated MCP-1 expression are likely engaged with slower kinetics.

HIF1-α has emerged as one of the central regulators of LPS-induced inflammation (41). LPS slowly, but strongly induced HIF-1α protein expression in macrophages, and its expression was correlated with proinflammatory cytokine secretions (42). Recent findings indicated that HIF-1α-induced glycolytic adaptation is essential to cytokine production in activated macrophages (43). In this study, we identified PDE10A is a critical regulator of LPS-induced HIF-1α expression. HIF-1α also plays important roles in vascular inflammation and heart failure (44). These results were consistent with our RNA-Seq data in the whole heart after chronic injury (20). It is known that HIF-1 α mediates the metabolic adaptation to LPS stimulation, and regulates the transition from oxidative to glycolytic metabolism (45, 46). Such shift in metabolism is essential to provide energy and redox balance for sustained cytokine production (30). In this study, both TP-10 and IDF-11774 treatments decreased LPS-induced MCP-1 production in PDE10A-WT macrophages, but IDF-11774 treatment had no more effect on MCP-1 production in PDE10A-KO cells or TP-10 treated cells. Previous studies have indicated that HIF-1α regulates MCP-1 at the transcriptional level (13), and HIF-1α expression is associated with MCP-1 expression in lung inflammation (47). It is possible that PDE10A mediated MCP-1 production through a combination of metabolic programming, of which HIF-1α is one.

To determine the role of PDE10A in lung inflammation in vivo, we used LPS exposure by oropharyngeal delivery and inhalation in mice. With oropharyngeal delivery, the acute dose of LPS delivered to the lungs of each mice can be assured. Airborne LPS provides physiological dose rate of LPS with relatively even distribution within the alveolar region (48). In this study, by using global PDE10A knockout mice, PDE10A deficiency can significantly reduce lung inflammation in two different delivery routes (Fig. 5 and 6). Furthermore, with systemic application of PDE10A inhibitor TP-10, we obtained similar results that PDE10A deficiency and activity inhibition significantly suppressed the

expression of inflammatory molecules such as MCP-1, IL-6, and IL-1β in the lung and the BAL fluid as well as inhibited inflammatory cell infiltration into the lung (Fig. 6 and 7). Increased neutrophil numbers, as well as high MPO and cytokine levels in BAL fluid are hallmarks of the inflammatory response in ALI. Interestingly, recent genome-wide association studies (GWAS) indicated that PDE10A is a candidate gene for asthma in mice and human (49, 50) as well as smoking-induced lung cancer (51). Thus, our current findings together with previous reports suggest a critical role of PDE10A induction in pulmonary pathology. The precise function of macrophage PDE10A in lung inflammation remains to be determined in the future by developing a macrophage-specific PDE10A knockout mouse.

Tissue damaged by injury leads to increased vascular permeability that triggers neutrophil and circulating macrophage infiltration, and excessive inflammation has detrimental effects on recovery after injury (52). Recent studies found PDE10A was acutely up-regulated in brain in a severity-dependent manner by traumatic brain injury in rats (53) and by transient middle cerebral artery occlusion in mice (54). In addition to brain injury, our recent data showed that PDE10A expression was upregulated in both human and mouse failing hearts, and PDE10A deficiency or inhibition by TP-10 attenuated stress-induced cardiac remodeling and dysfunction (20). The precise role of PDE10A in tissue injury following macrophage and neutrophil-mediated inflammation requires further study.

The PDE4 inhibitor, roflumilast, reduces exacerbation rates in severe COPD patients with chronic bronchitis and is currently approved by Food and Drug Administration (FDA) (9). However, the clinical dosage and efficacy of roflumilast is limited by target-related side effects, such as nausea, diarrhea and weight loss that make it intolerable for some patients (55). Several PDE10A inhibitors have been administered systemically in clinical trials and proved to be safe in humans (56). However, the development of PDE10A inhibitors that do not cross the blood brain barrier is necessary for targeting PDE10A in peripheral diseases because currently available PDE10 inhibitors are known to cross the blood brain barrier. Indeed, we observed sedation in mice with TP-10 injection, but the behavior change appeared to last for a short period of time and mice remained active without apparent abnormality at the time of sacrifice. PDE10A inhibitors with lower brain penetration have been recently discovered (57). New data suggest that inhibition of multiple PDEs is necessary to increase intracellular cAMP and the PDE-regulated phosphoproteome (58). We believe that developing novel therapeutic strategies based on PDE10A inhibition or combination therapy with PDE4B and PDE10A inhibition may be of great interest for ameliorating lung inflammation. These findings show for the first time that PDE10A plays a critical role in lung inflammation by promoting the activation of resident macrophages and infiltration of neutrophils. Future studies using more pathologic stimulators of ALI will be required to determine the magnitude of inhibition of PDE10A necessary to achieve a beneficial result.

Supplementary Material

Refer to Web version on PubMed Central for supplementary material.

Support statement:

This work was financially supported by National Institute of Health HL134910 (to B.C.B. and C.Y.).

References

1. Bellani G, Laffey JG, Pham T, Fan E, Brochard L, Esteban A, Gattinoni L, van Haren F, Larsson A, McAuley DF, Ranieri M, Rubenfeld G, Thompson BT, Wrigge H, Slutsky AS, Pesenti A, L. S. Investigators, and E. T. Group. 2016. Epidemiology, Patterns of Care, and Mortality for Patients With Acute Respiratory Distress Syndrome in Intensive Care Units in 50 Countries. JAMA 315: 788–800. [PubMed: 26903337]
2. Maca J, Jor O, Holub M, Sklienka P, Bursa F, Burda M, Janout V, and Sevcik P. 2017. Past and Present ARDS Mortality Rates: A Systematic Review. Respir Care 62: 113–122. [PubMed: 27803355]
3. Matthay MA, and Zemans RL. 2011. The acute respiratory distress syndrome: pathogenesis and treatment. Annu Rev Pathol 6: 147–163. [PubMed: 20936936]
4. Newton AC, Bootman MD, and Scott JD. 2016. Second Messengers. Cold Spring Harb Perspect Biol 8.
5. Maurice DH, Ke H, Ahmad F, Wang Y, Chung J, and Manganiello VC. 2014. Advances in targeting cyclic nucleotide phosphodiesterases. Nat Rev Drug Discov 13: 290–314. [PubMed: 24687066]
6. Movsesian M, Ahmad F, and Hirsch E. 2018. Functions of PDE3 Isoforms in Cardiac Muscle. J Cardiovasc Dev Dis 5.
7. Mongillo M, McSorley T, Evellin S, Sood A, Lissandron V, Terrin A, Huston E, Hannawacker A, Lohse MJ, Pozzan T, Houslay MD, and Zaccolo M. 2004. Fluorescence resonance energy transfer-based analysis of cAMP dynamics in live neonatal rat cardiac myocytes reveals distinct functions of compartmentalized phosphodiesterases. Circ Res 95: 67–75. [PubMed: 15178638]
8. Page CP, and Spina D. 2012. Selective PDE inhibitors as novel treatments for respiratory diseases. Curr Opin Pharmacol 12: 275–286. [PubMed: 22497841]
9. Garnock-Jones KP 2015. Roflumilast: A Review in COPD. Drugs 75: 1645–1656. [PubMed: 26338438]
10. Keating GM 2017. Apremilast: A Review in Psoriasis and Psoriatic Arthritis. Drugs 77: 459–472. [PubMed: 28213862]
11. Soderling SH, Bayuga SJ, and Beavo JA. 1999. Isolation and characterization of a dual-substrate phosphodiesterase gene family: PDE10A. Proc Natl Acad Sci U S A 96: 7071–7076. [PubMed: 10359840]
12. Fujishige K, Kotera J, Michibata H, Yuasa K, Takebayashi S, Okumura K, and Omori K. 1999. Cloning and characterization of a novel human phosphodiesterase that hydrolyzes both cAMP and cGMP (PDE10A). J Biol Chem 274: 18438–18445. [PubMed: 10373451]
13. Lee YY, Park JS, Leem YH, Park JE, Kim DY, Choi YH, Park EM, Kang JL, and Kim HS. 2019. The phosphodiesterase 10 inhibitor papaverine exerts anti-inflammatory and neuroprotective effects via the PKA signaling pathway in neuroinflammation and Parkinson's disease mouse models. J Neuroinflammation 16: 246. [PubMed: 31791357]
14. Wilson LS, and Brandon NJ. 2015. Emerging biology of PDE10A. Curr Pharm Des 21: 378–388. [PubMed: 25159072]
15. Schmidt CJ, Chapin DS, Cianfrogna J, Corman ML, Hajos M, Harms JF, Hoffman WE, Lebel LA, McCarthy SA, Nelson FR, Proulx-LaFrance C, Majchrzak MJ, Ramirez AD, Schmidt K, Seymour PA, Siuciak JA, Tingley FD 3rd, Williams RD, Verhoest PR, and Menniti FS. 2008. Preclinical characterization of selective phosphodiesterase 10A inhibitors: a new therapeutic approach to the treatment of schizophrenia. J Pharmacol Exp Ther 325: 681–690. [PubMed: 18287214]
16. Beaumont V, Zhong S, Lin H, Xu W, Bradaia A, Steidl E, Gleyzes M, Wadel K, Buisson B, Padovan-Neto FE, Chakroborty S, Ward KM, Harms JF, Beltran J, Kwan M, Ghavami A, Haggkvist J, Toth M, Halldin C, Varrone A, Schaab C, Dybowski JN, Elschenbroich S, Lehtimaki K, Heikkinen T, Park L, Rosinski J, Mrzljak L, Lavery D, West AR, Schmidt CJ, Zaleska MM,

and Munoz-Sanjuan I. 2016. Phosphodiesterase 10A Inhibition Improves Cortico-Basal Ganglia Function in Huntington's Disease Models. Neuron 92: 1220–1237. [PubMed: 27916455]

17. Lee K, Lindsey AS, Li N, Gary B, Andrews J, Keeton AB, and Piazza GA. 2016. beta-catenin nuclear translocation in colorectal cancer cells is suppressed by PDE10A inhibition, cGMP elevation, and activation of PKG. Oncotarget 7: 5353–5365. [PubMed: 26713600]
18. Zhu B, Lindsey A, Li N, Lee K, Ramirez-Alcantara V, Canzoneri JC, Fajardo A, Madeira da Silva L, Thomas M, Piazza JT, Yet L, Eberhardt BT, Gurpinar E, Otali D, Grizzle W, Valiyaveettil J, Chen X, Keeton AB, and Piazza GA. 2017. Phosphodiesterase 10A is overexpressed in lung tumor cells and inhibitors selectively suppress growth by blocking beta-catenin and MAPK signaling. Oncotarget 8: 69264–69280. [PubMed: 29050202]
19. Li N, Lee K, Xi Y, Zhu B, Gary BD, Ramirez-Alcantara V, Gurpinar E, Canzoneri JC, Fajardo A, Sigler S, Piazza JT, Chen X, Andrews J, Thomas M, Lu W, Li Y, Laan DJ, Moyer MP, Russo S, Eberhardt BT, Yet L, Keeton AB, Grizzle WE, and Piazza GA. 2015. Phosphodiesterase 10A: a novel target for selective inhibition of colon tumor cell growth and beta-catenin-dependent TCF transcriptional activity. Oncogene 34: 1499–1509. [PubMed: 24704829]
20. Chen S, Zhang Y, Lighthouse JK, Mickelsen DM, Wu J, Yao P, Small EM, and Yan C. 2020. A Novel Role of Cyclic Nucleotide Phosphodiesterase 10A in Pathological Cardiac Remodeling and Dysfunction. Circulation 141: 217–233. [PubMed: 31801360]
21. Slavin SA, Leonard A, Grose V, Fazal F, and Rahman A. 2018. Autophagy inhibitor 3-methyladenine protects against endothelial cell barrier dysfunction in acute lung injury. Am J Physiol Lung Cell Mol Physiol 314: L388–L396. [PubMed: 29074492]
22. Zhang X, Goncalves R, and Mosser DM. 2008. The isolation and characterization of murine macrophages. Curr Protoc Immunol Chapter 14: Unit 14 11.
23. Mukhopadhyay S, Pluddemann A, Hoe JC, Williams KJ, Varin A, Makepeace K, Aknin ML, Bowdish DM, Smale ST, Barclay AN, and Gordon S. 2010. Immune inhibitory ligand CD200 induction by TLRs and NLRs limits macrophage activation to protect the host from meningococcal septicemia. Cell Host Microbe 8: 236–247. [PubMed: 20833375]
24. Xue C, Sowden M, and Berk BC. 2017. Extracellular Cyclophilin A, Especially Acetylated, Causes Pulmonary Hypertension by Stimulating Endothelial Apoptosis, Redox Stress, and Inflammation. Arterioscler Thromb Vasc Biol 37: 1138–1146. [PubMed: 28450293]
25. Zhang C, Hsu CG, Mohan A, Shi H, Li D, and Yan C. 2020. Vinpocetine protects against the development of experimental abdominal aortic aneurysms. Clin Sci (Lond) 134: 2959–2976. [PubMed: 33111936]
26. Laskin DL, Malaviya R, and Laskin JD. 2019. Role of Macrophages in Acute Lung Injury and Chronic Fibrosis Induced by Pulmonary Toxicants. Toxicol Sci 168: 287–301. [PubMed: 30590802]
27. Jarjour NN, Schwarzkopf EA, Bradstreet TR, Shchukina I, Lin CC, Huang SC, Lai CW, Cook ME, Taneja R, Stappenbeck TS, Randolph GJ, Artyomov MN, Urban JF Jr., and Edelson BT. 2019. Bhlhe40 mediates tissue-specific control of macrophage proliferation in homeostasis and type 2 immunity. Nat Immunol 20: 687–700. [PubMed: 31061528]
28. Shi H, Wang Y, Li X, Zhan X, Tang M, Fina M, Su L, Pratt D, Bu CH, Hildebrand S, Lyon S, Scott L, Quan J, Sun Q, Russell J, Arnett S, Jurek P, Chen D, Kravchenko VV, Mathison JC, Moresco EM, Monson NL, Ulevitch RJ, and Beutler B. 2016. NLRP3 activation and mitosis are mutually exclusive events coordinated by NEK7, a new inflammasome component. Nat Immunol 17: 250–258. [PubMed: 26642356]
29. Peyssonnaux C, Cejudo-Martin P, Doedens A, Zinkernagel AS, Johnson RS, and Nizet V. 2007. Cutting edge: Essential role of hypoxia inducible factor-1alpha in development of lipopolysaccharide-induced sepsis. J Immunol 178: 7516–7519. [PubMed: 17548584]
30. Tannahill GM, Curtis AM, Adamik J, Palsson-McDermott EM, McGettrick AF, Goel G, Frezza C, Bernard NJ, Kelly B, Foley NH, Zheng L, Gardet A, Tong Z, Jany SS, Corr SC, Haneklaus M, Caffrey BE, Pierce K, Walmsley S, Beasley FC, Cummins E, Nizet V, Whyte M, Taylor CT, Lin H, Masters SL, Gottlieb E, Kelly VP, Clish C, Auron PE, Xavier RJ, and O'Neill LA. 2013. Succinate is an inflammatory signal that induces IL-1beta through HIF-1alpha. Nature 496: 238–242. [PubMed: 23535595]

31. Matute-Bello G, Frevert CW, and Martin TR. 2008. Animal models of acute lung injury. Am J Physiol Lung Cell Mol Physiol 295: L379–399. [PubMed: 18621912]
32. Lazarevic-Pasti T, Leskovac A, and Vasic V. 2015. Myeloperoxidase Inhibitors as Potential Drugs. Curr Drug Metab 16: 168–190. [PubMed: 26279325]
33. Lea S, Metryka A, Li J, Higham A, Bridgewood C, Villetti G, Civelli M, Facchinetti F, and Singh D. 2019. The modulatory effects of the PDE4 inhibitors CHF6001 and roflumilast in alveolar macrophages and lung tissue from COPD patients. Cytokine 123: 154739. [PubMed: 31319374]
34. Gerlo S, Kooijman R, Beck IM, Kolmus K, Spooren A, and Haegeman G. 2011. Cyclic AMP: a selective modulator of NF-kappaB action. Cell Mol Life Sci 68: 3823–3841. [PubMed: 21744067]
35. Tasken K, and Aandahl EM. 2004. Localized effects of cAMP mediated by distinct routes of protein kinase A. Physiol Rev 84: 137–167. [PubMed: 14715913]
36. Bourne HR, Lichtenstein LM, Melmon KL, Henney CS, Weinstein Y, and Shearer GM. 1974. Modulation of inflammation and immunity by cyclic AMP. Science 184: 19–28. [PubMed: 4131281]
37. Siuciak JA, Chapin DS, Harms JF, Lebel LA, McCarthy SA, Chambers L, Shrikhande A, Wong S, Menniti FS, and Schmidt CJ. 2006. Inhibition of the striatum-enriched phosphodiesterase PDE10A: a novel approach to the treatment of psychosis. Neuropharmacology 51: 386–396. [PubMed: 16780899]
38. Torremans A, Ahnaou A, Van Hemelrijck A, Straetemans R, Geys H, Vanhoof G, Meert TF, and Drinkenburg WH. 2010. Effects of phosphodiesterase 10 inhibition on striatal cyclic AMP and peripheral physiology in rats. Acta Neurobiol Exp (Wars) 70: 13–19. [PubMed: 20407482]
39. Muller JM, Ziegler-Heitbrock HW, and Baeuerle PA. 1993. Nuclear factor kappa B, a mediator of lipopolysaccharide effects. Immunobiology 187: 233–256. [PubMed: 8330898]
40. Susuki-Miyata S, Miyata M, Lee BC, Xu H, Kai H, Yan C, and Li JD. 2015. Cross-talk between PKA-Cbeta and p65 mediates synergistic induction of PDE4B by roflumilast and NTHi. Proc Natl Acad Sci U S A 112: E1800–1809. [PubMed: 25831493]
41. Corcoran SE, and O'Neill LA. 2016. HIF1alpha and metabolic reprogramming in inflammation. J Clin Invest 126: 3699–3707. [PubMed: 27571407]
42. Blouin CC, Page EL, Soucy GM, and Richard DE. 2004. Hypoxic gene activation by lipopolysaccharide in macrophages: implication of hypoxia-inducible factor 1alpha. Blood 103: 1124–1130. [PubMed: 14525767]
43. Wang T, Liu H, Lian G, Zhang SY, Wang X, and Jiang C. 2017. HIF1alpha-Induced Glycolysis Metabolism Is Essential to the Activation of Inflammatory Macrophages. Mediators Inflamm 2017: 9029327. [PubMed: 29386753]
44. Semenza GL 2014. Hypoxia-inducible factor 1 and cardiovascular disease. Annu Rev Physiol 76: 39–56. [PubMed: 23988176]
45. Kelly B, and O'Neill LA. 2015. Metabolic reprogramming in macrophages and dendritic cells in innate immunity. Cell Res 25: 771–784. [PubMed: 26045163]
46. Lin N, and Simon MC. 2016. Hypoxia-inducible factors: key regulators of myeloid cells during inflammation. J Clin Invest 126: 3661–3671. [PubMed: 27599290]
47. Baay-Guzman GJ, Bebenek IG, Zeidler M, Hernandez-Pando R, Vega MI, Garcia-Zepeda EA, Antonio-Andres G, Bonavida B, Riedl M, Kleerup E, Tashkin DP, Hankinson O, and Huerta-Yepez S. 2012. HIF-1 expression is associated with CCL2 chemokine expression in airway inflammatory cells: implications in allergic airway inflammation. Respir Res 13: 60. [PubMed: 22823210]
48. Driscoll KE, Costa DL, Hatch G, Henderson R, Oberdorster G, Salem H, and Schlesinger RB. 2000. Intratracheal instillation as an exposure technique for the evaluation of respiratory tract toxicity: uses and limitations. Toxicol Sci 55: 24–35. [PubMed: 10788556]
49. Melen E, Kho AT, Sharma S, Gaedigk R, Leeder JS, Mariani TJ, Carey VJ, Weiss ST, and Tantisira KG. 2011. Expression analysis of asthma candidate genes during human and murine lung development. Respir Res 12: 86. [PubMed: 21699702]
50. Melen E, Himes BE, Brehm JM, Boutaoui N, Klanderman BJ, Sylvia JS, and Lasky-Su J. 2010. Analyses of shared genetic factors between asthma and obesity in children. J Allergy Clin Immunol 126: 631–637 e631–638. [PubMed: 20816195]

51. Fusco JP, Pita G, Pajares MJ, Andueza MP, Patino-Garcia A, de-Torres JP, Gurpide A, Zulueta J, Alonso R, Alvarez N, Pio R, Melero I, Sanmamed MF, Rodriguez Ruiz M, Gil-Bazo I, Lopez-Picazo JM, Casanova C, Baz Davila R, Agudo A, Lozano MD, Gonzalez A, Sala N, Ardanaz E, Benitez J, Montuenga L, Gonzalez-Neira A, and Perez-Gracia JL. 2018. Genomic characterization of individuals presenting extreme phenotypes of high and low risk to develop tobacco-induced lung cancer. Cancer Med.
52. Wynn TA, and Vannella KM. 2016. Macrophages in Tissue Repair, Regeneration, and Fibrosis. Immunity 44: 450–462. [PubMed: 26982353]
53. Song H, Fang S, Gao J, Wang J, Cao Z, Guo Z, Huang Q, Qu Y, Zhou H, and Yu J. 2018. Quantitative Proteomic Study Reveals Up-Regulation of cAMP Signaling Pathway-Related Proteins in Mild Traumatic Brain Injury. J Proteome Res 17: 858–869. [PubMed: 29215295]
54. Ito M, Aswendt M, Lee AG, Ishizaka S, Cao Z, Wang EH, Levy SL, Smerin DL, McNab JA, Zeineh M, Leuze C, Goubran M, Cheng MY, and Steinberg GK. 2018. RNA-Sequencing Analysis Revealed a Distinct Motor Cortex Transcriptome in Spontaneously Recovered Mice After Stroke. Stroke; a journal of cerebral circulation 49: 2191–2199.
55. Chong J, Leung B, and Poole P. 2017. Phosphodiesterase 4 inhibitors for chronic obstructive pulmonary disease. Cochrane Database Syst Rev 9: CD002309. [PubMed: 28922692]
56. Zagorska A, Partyka A, Bucki A, Gawalska A, Czopek A, and Pawlowski M. 2018. Phosphodiesterase 10 Inhibitors - Novel Perspectives for Psychiatric and Neurodegenerative Drug Discovery. Current medicinal chemistry.
57. Kadoh Y, Miyoshi H, Matsumura T, Tanaka Y, Hongu M, Kimura M, Takedomi K, Omori K, Kotera J, Sasaki T, Kobayashi T, Taniguchi H, Watanabe Y, Kojima K, Sakamoto T, Himiyama T, and Kawanishi E. 2018. Discovery of 2-[(E)-2-(7-Fluoro-3-methylquinoxalin-2-yl)vinyl]-6-pyrrolidin-1-yl-N-(tetrahydro -2H-pyran-4-yl)pyrimidin-4-amine Hydrochloride as a Highly Selective PDE10A Inhibitor. Chem Pharm Bull (Tokyo) 66: 243–250. [PubMed: 29491258]
58. Beltejar MG, Lau HT, Golkowski MG, Ong SE, and Beavo JA. 2017. Analyses of PDE-regulated phosphoproteomes reveal unique and specific cAMP-signaling modules in T cells. Proc Natl Acad Sci U S A 114: E6240–E6249. [PubMed: 28634298]

KEY POINTS

- LPS induces PDE10A up-regulation in macrophages in vitro and in lung tissues.
- PDE10A regulates MCP-1 production in macrophages.
- PDE10A inhibition reduces lung inflammation in mouse models of LPS exposure.

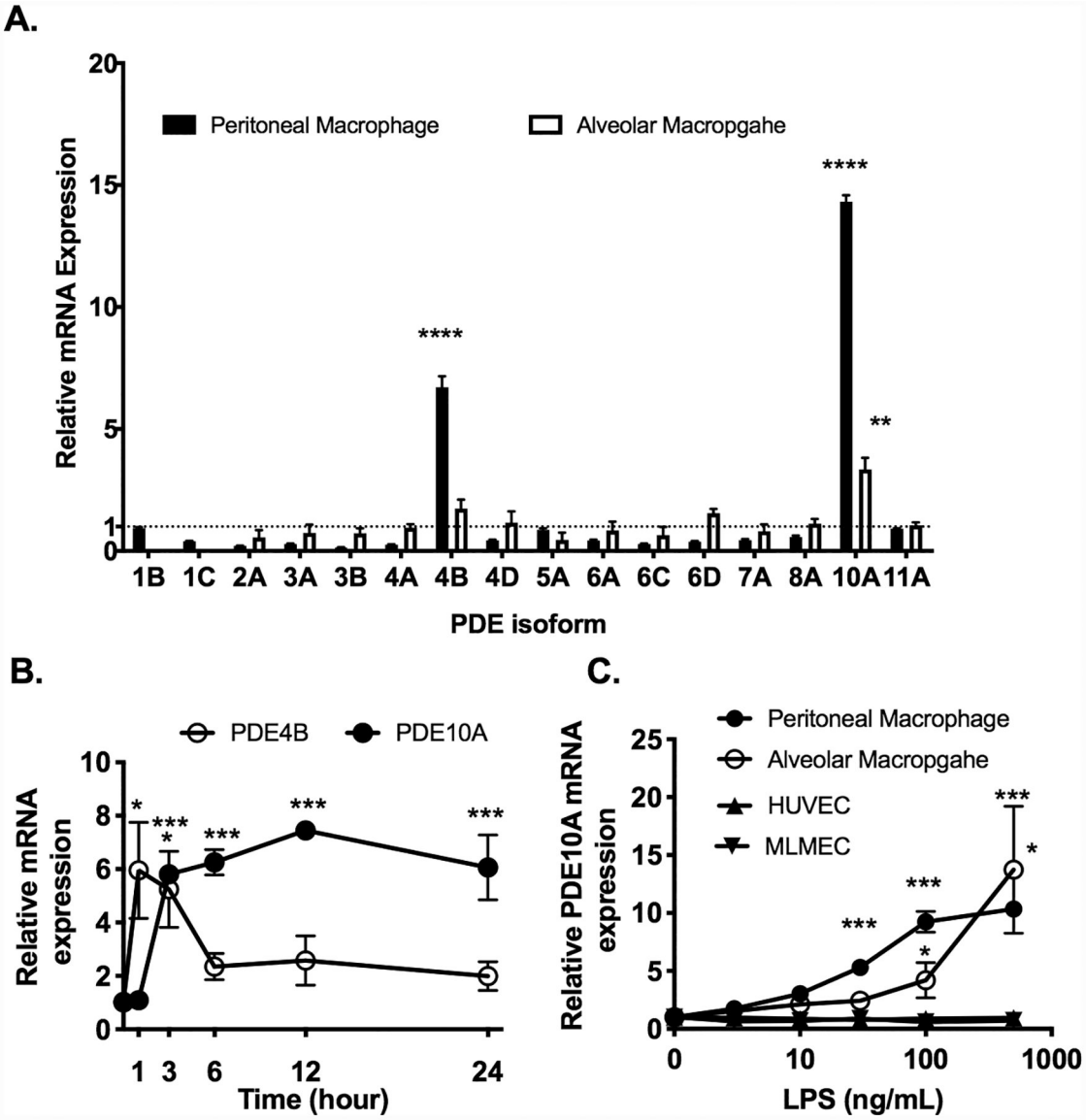

FIGURE 1. LPS increases PDE10A gene expression in vitro macrophages.

(A) Different PDE expressions after LPS (100ng/mL) stimulation for 6 hours in peritoneal macrophages (Black bar) and alveolar macrophages (White Bar), dashed line: no LPS. (B) Time course of PDE4B and PDE10A gene expression after LPS (100ng/mL) treatment in peritoneal macrophages. PDE4B (Open circle) and PDE10A (Closed circle) (C) Dose response of PDE10A gene expression after LPS stimulation for 6 hours in macrophages or endothelial cells. Statistics in A were performed using multiple T-tests. Statistics in B-C were performed using a one-way ANOVA and Bonferroni's post hoc test. Values that were significantly different between the LPS-and no LPS-treated groups. *P <0.05, **P < 0.01, ****P < 0.0001. Data represent the mean ± SEM.

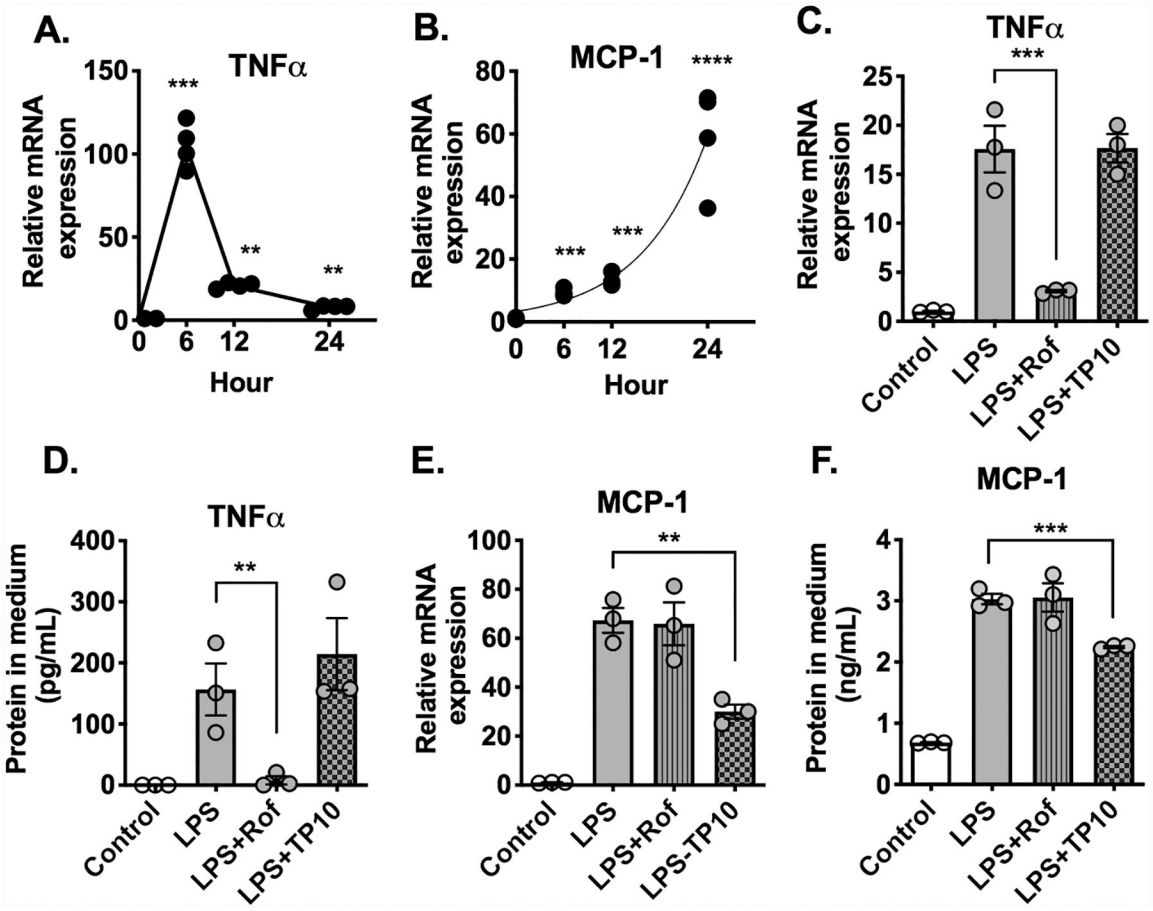

FIGURE 2. PDE10A and PDE4 inhibition differentially regulate MCP-1 and TNFa expression in macrophages after LPS stimulation.

Peritoneal macrophages were stimulated with LPS(100ng/mL) for the indicated time periods. Cell lysates were used for measuring gene expression. (A) Time course of TNFα gene expression (B) Time course of MCP-1 gene expression. Samples were harvested after 24 hour LPS (100ng/mL) stimulation in peritoneal macrophages incubated with or without TP-10 (1μM) or Roflumilast (Rof, 1μM). (C) TNFα gene expression in cell lysate (D) TNFα secretion in medium (E) MCP-1 gene expression in cell lysate (F) MCP-1 secretion in medium. Statistics in A-F were performed using a one-way ANOVA and Bonferroni's post hoc test. *P < 0.05, **P < 0.01, ***P<0.001, Data represent the mean ± SEM.

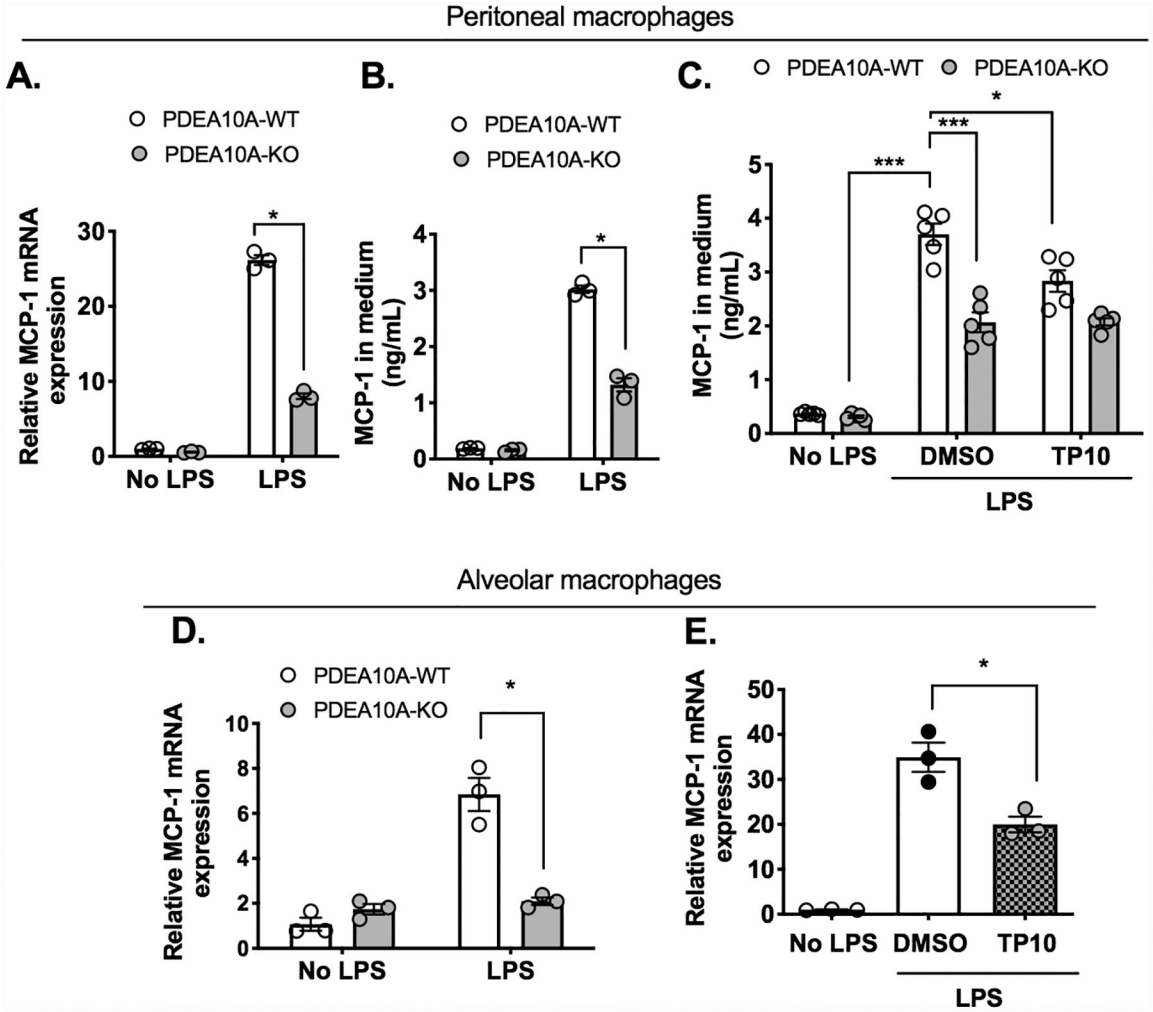

FIGURE 3. PDE10A inhibition or knockout reduces MCP-1 expression and secretion in macrophages after LPS treatment.

(A) MCP-1 gene expression in cell lysate and (B-C) protein secretion in the medium after LPS (100ng/mL) stimulation in PDE10A-WT and PDE10A-KO peritoneal macrophages with or without TP-10 (1μM) treatment. (D) MCP-1 gene expression after LPS stimulation for 24 hours in PDE10A-WT and PDE10A-KO alveolar macrophages. PDE10A-WT : white circle and PDE10A-KO : gray circle. (E) MCP-1 gene expression after LPS stimulation in PDE10A-WT alveolar macrophage with DMSO or TP-10 (1μM) treatment. Statistics in A,B,C,D were performed using a 2-way ANOVA and Bonferroni's post hoc test. Statistics in E were performed using a one-way ANOVA and Bonferroni's post hoc test. *P < 0.05, ***P<0.001, Data represent the mean ± SEM.

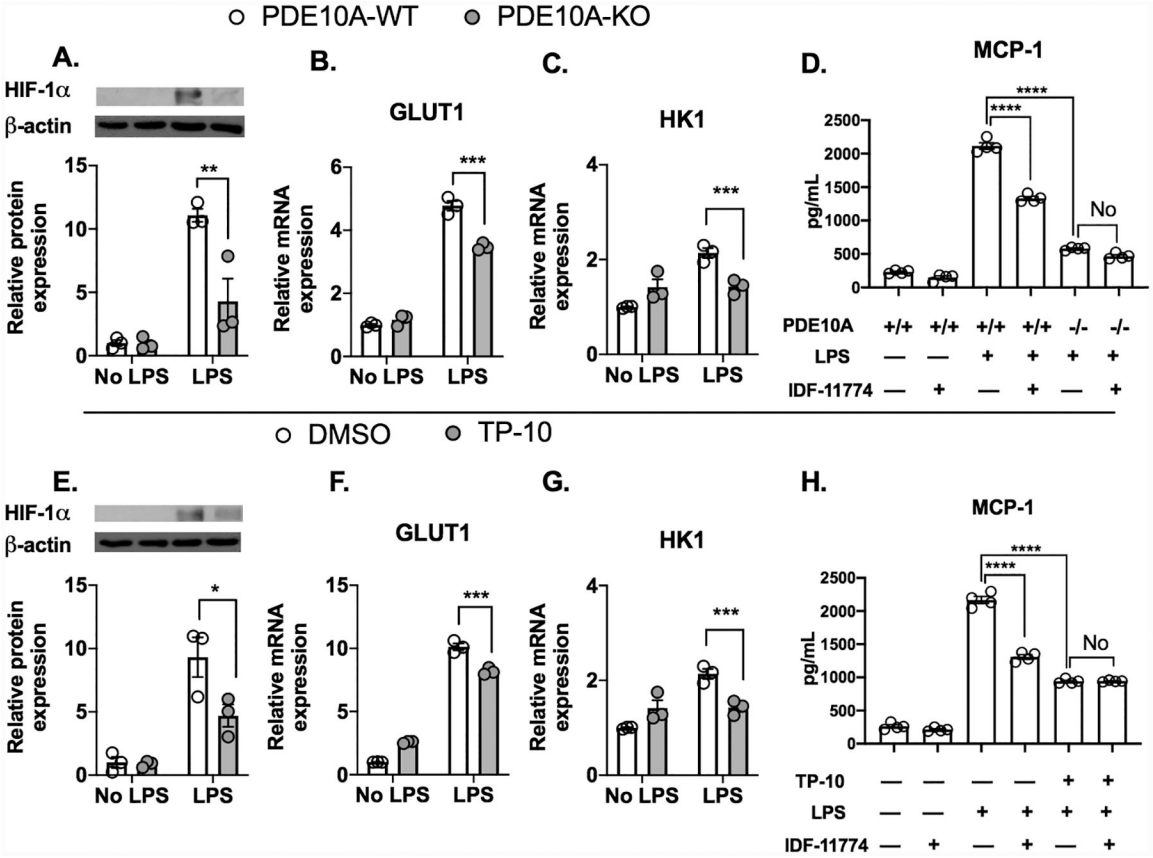

FIGURE 4. PDE10A inhibition or knockout reduces HIF-1α expression in macrophages after LPS treatment.

(A) HIF-1α protein expression (B) GLUT1 mRNA expression (C) HK1 mRNA expression after LPS stimulation for 24 hr in PDE10A-WT and PDE10A-KO peritoneal macrophages. (D) MCP-1 secretion after LPS stimulation with or without HIF-1 α inhibitor (IDF-11774, 12 μM) for 24 hours in PDE10A-WT or PDE10A-KO peritoneal macrophages. Peritoneal macrophages were stimulated with LPS and co-incubated with DMSO or TP-10 (1μM) for 24 hr. (E) HIF-1α protein expression (F) GLUT1 mRNA expression (G) HK1 mRNA expression (H) MCP-1 secretion after LPS stimulation with DMSO, TP-10 (1μM), or IDF-11774 (12 μM) for 24 hr in peritoneal macrophages. Statistics in A-C, and E-G were performed using a 2-way ANOVA and Bonferroni's post hoc test. Statistics in D and H were performed using a one-way ANOVA and Bonferroni's post hoc test. *P < 0.05, ***P<0.001, Data represent the mean ± SEM.

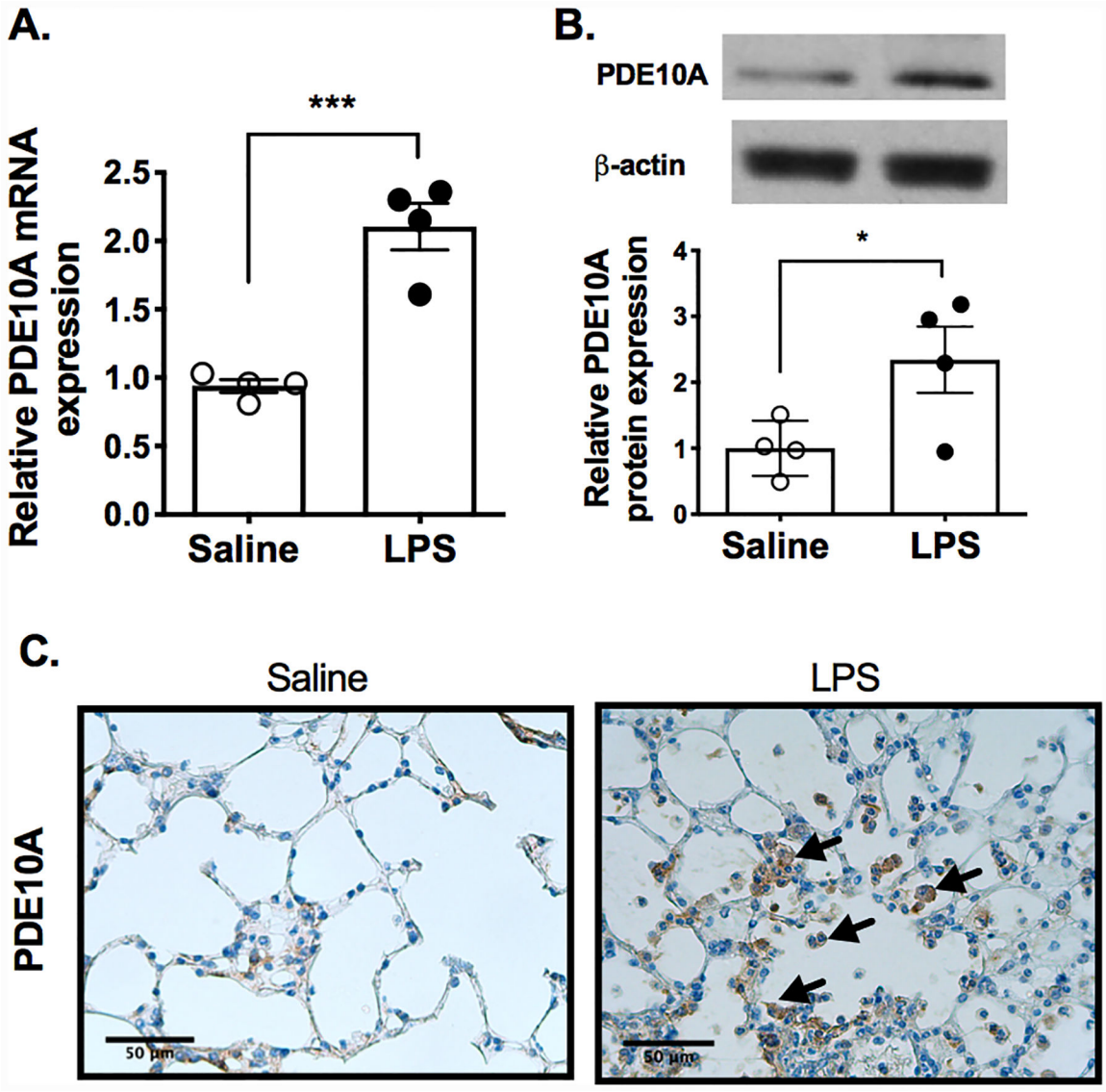

FIGURE 5. LPS exposure increases PDE10A gene and protein expression in lung.

Male C57BL/6J mice underwent acute LPS (10mg) or saline (10mL) exposure for 30min. Lung tissues were harvested for (A) PDE10A gene expression at 6 hours post exposure normalized to b-actin (B) PDE10A protein expression at 6 hours post exposure (C) PDE10A staining at 24 hours following oropharyngeal delivery of 0.9% saline (50 μL) or LPS (0.2mg/kg) (Arrowheads indicate PDE10A positive cells, original magnification, x400); N=4 mice from each group; Saline (open circles), LPS (close circles). All data are expressed as mean ± SEM, Statistics in A and B were performed using a paired t test. **P<0.01.

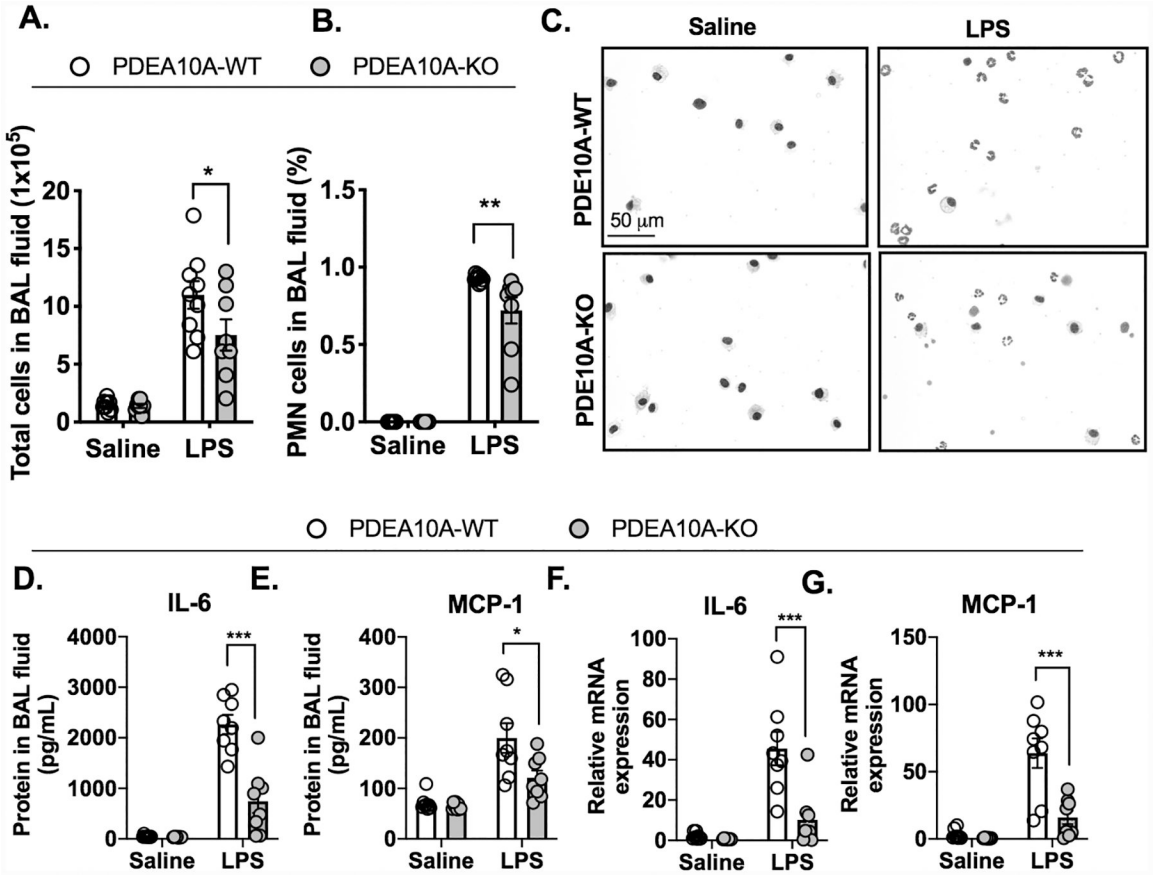

FIGURE 6. PDE10A knockout reduces lung inflammation after LPS delivery by oropharyngeal aspiration in mice.

After oropharyngeal administration of LPS (0.2 mg/kg) or saline (50 μL) in male and female PDE10A-WT or PDE10A-KO mice, BAL fluid and lung tissues were harvested at 24 hours post treatment. A) Total cell number, (B) quantification of polymorphonuclear neutrophils (PMN) percentage in BAL fluid and (C) reprehensive of cytospots of BAL fluid after HEMA 3 Staining (magnification, x400). Cell densities of the cytospin preparations were normalized among each group. (D) IL-6 and (E) MCP-1 secretion in BAL fluid; (F) IL-6 and (G) MCP-1 mRNA expression in lung tissue. PDE10A-WT (white circle) and PDE10A-KO (gray circle) mice. (N=8, 4 male and 4 female mice for each group). All data were expressed as mean ± SEM, Statistics were performed using a 2-way ANOVA and Bonferroni's post hoc test. *P<0.05, **P<0.01, ****P<0.001 between LPS-WT and LPS-KO groups.

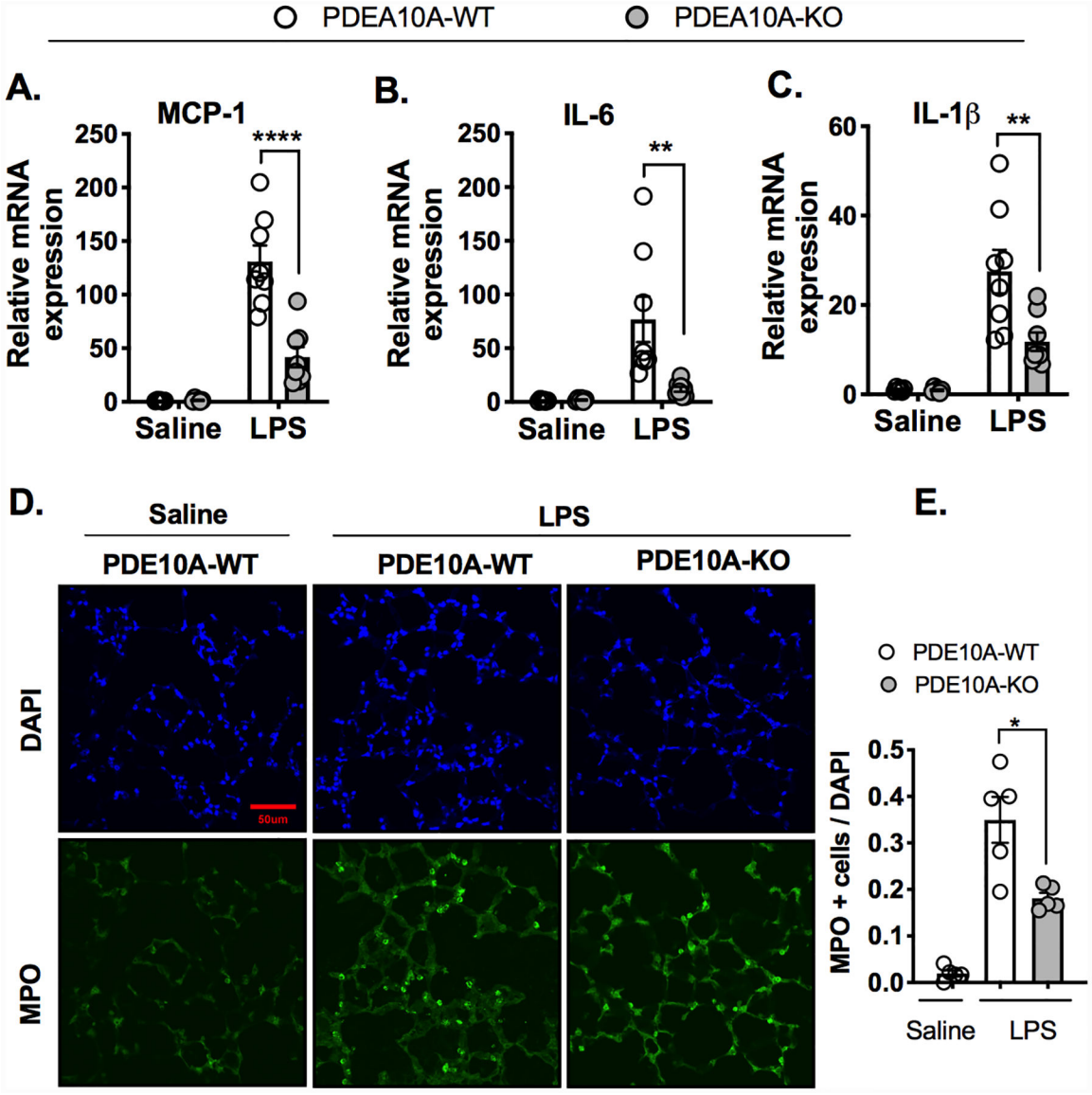

FIGURE 7.

PDE10A knockout reduces lung inflammation after LPS inhalation in mice. PDE10A-WT or PDE10A-KO mice were exposed to LPS (10mg) or saline (10mL) exposure aerosol for 30 min, and samples were analyzed at 24 hours post exposure. (A) MCP-1, (B) IL-6, and (C) IL-1β mRNA expression in lung tissue. N=6 (3male, 3 female) for each saline-exposed group and N= 8 (4 male, 4 female) for each LPS-exposed group. In a separate experiment, lung tissues were harvested from male PDE10A-WT or PDE10A-KO male mice at 24 hours after LPS exposure. (D) Immunofluorescence of representative lung sections for MPO staining at 24 hours post LPS exposure. Green: MPO positive cells; Blue: DAPI, Magnification, x400. (E) Quantification of MPO-positive cells / DAPI. (magnification, x400). PDE10A-WT (white circle) and PDE10A-KO (gray circle) mice. N=5 for each group. Data were expressed as mean ± SEM. Statistics in A, B, C were performed using a 2-way ANOVA and Bonferroni's post hoc test. Statistics in E were performed using a

one-way ANOVA and Bonferroni's post hoc test. *P<0.05, **P<0.01, ****P<0.001 between LPS-WT and LPS-KO groups.

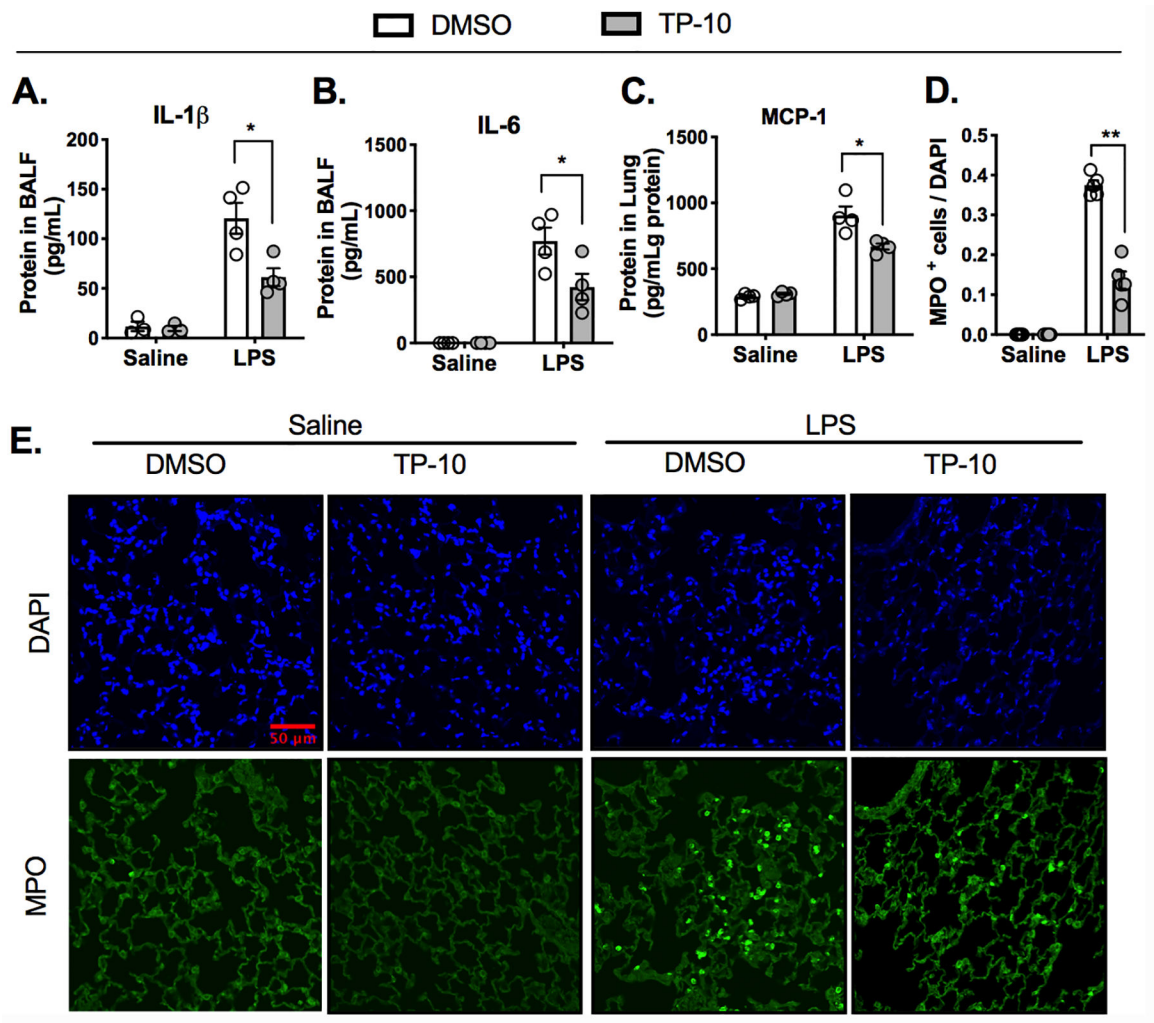

FIGURE 8.

PDE10A inhibition by TP-10 reduces LPS-induced lung inflammation. PDE10A-WT male mice were exposed to LPS (10mg) or saline (10mL) aerosol and samples were analyzed at 6 hours post exposure. (A) Secretion of IL-1β , and (B) IL-6 from BAL Fluid and (C) Protein expression of MCP-1 in lung (n=4 from each group). In a separate experiment, lung tissues were harvested from PDE10A-WT male mice at 24 hours after LPS exposure. (D) Quantification of MPO-positive cells/ DAPI. Vehicle treated (white circle) and TP-10 (6mg/kg) treated (gray circle) (n=4 from each saline groups and n=5 from each LPS group). (E) Immunofluorescence of representative lung sections for MPO positive staining (green) at 24 hours post exposure. Magnification, x400. Statistics in A-D were performed using a 2-way ANOVA and Bonferroni's post hoc test. *P < 0.05. All data were represented as mean ± SEM.

TABLE 1.

Cytokine and chemokine protein expression in lung tissue and secretion in BAL fluid after LPS inhalation in mice.

	Lung tissue (pg/mg protein)				BALF (pg/mL)			
	Saline		LPS		Saline		LPS	
	PDE10A-WT	PDE10A-KO	PDE10A-WT	PDE10A-KO	PDE10A-WT	PDE10A-KO	PDE10A-WT	PDE10A-KO
MCP-1	22.99±4.76	35.87±8.07	407.94±33.71#	158.92±13.58*	NA	NA	156.32±10.06#	15.46±3.12*
IL-6	0.82±0.11	0.93±0.05	126.37±15.28#	33.49±1.58*	0.32±0.01	0.41±0.02	293.94±41.00#	146.76±13.17*
IL-1b	3.87±0.37	3.95±0.13	26.26±0.42#	14.01±0.62*	3.45±0.68	1.05	9.65±1.22#	6.46±0.58
TNFa	NA	0.14	7.73±0.36#	4.44±0.24*	0.12	NA	41.95±4.57#	36.4±3.84
GM-CSF	1.27±0.12	1.4±0.08	12.34±0.12	8.9±0.78	2.69±0.30	2.53±0.27	15.40±0.92#	9.37±1.31*
IL-10	0.69±0.03	0.76±0.07	0.87±0.07	0.7±0.05	0.36±0.06	0.69±0.11	0.36	0.17±0.01
IL-12	0.26±0.07	0.32±0.09	0.54±0.05	0.4±0.06	1.07±0.07	0.73±0.15	1.76±0.32	1.23±0.34*
IL-2	1.76±0.13	2.46±0.04	0.97±0.11	0.67±0.05	0.85±0.09	0.92±0.07	0.77±0.16	0.25±0.03
IL-4	0.3±0.02	0.29±0.02	0.16±0.01	0.2±0.01	0.14±0.01	0.13±0.01	025±0.03	0.24±0.01
IFNr	0.45±0.04	0.6±0.06	0.83±0.08#	0.22±0.03*	NA	NA	NA	NA

PDE10A-WT or PDE10A-KO mice were exposed to LPS (10mg) or saline aerosol for 30min, and samples were analyzed at 24 hours post exposure. N=3 for each group. All data were expressed as mean ± SEM, Statistics were performed using a 2-way ANOVA and Bonferroni's post hoc test.

# P<0.05, Saline-PDE10AWT vs. LPS-PDE10AWT group;

* P<0.05, LPS-PDE10A-WT vs. LPS-PDE10A-KO group.